MINERALOGICAL MAGAZINE, DECEMBER 1984, VOL. 48, PP. 481–94

The composition of diopside solid solutions, and of liquids, in equilibrium with forsterite, plagioclase, and liquid in the system Na_2O–CaO–MgO–Al_2O_3–SiO_2 and in remelted rocks from 1 bar to 12 kbar

GORDON M. BIGGAR

Department of Geology, University of Edinburgh, Edinburgh EH9 3JW

ABSTRACT. Subsolidus diopside compositions and coexisting diopside and liquid compositions which are also in equilibrium with anorthite and forsterite in the system CaO–MgO–Al_2O_3–SiO_2 were determined by X-ray diffraction and by electron microprobe in samples equilibrated at 1 bar and at 7 kbar. Along with previous data from the literature and using a recently published grid relating diffraction peaks to composition, results from both techniques are satisfactorily reconciled. At 1 bar, diopside composition (moles, Di = $CaMgSi_2O_6$, En = $Mg_2Si_2O_6$, CaTs = $CaAl_2SiO_6$) in equilibrium with anorthite, forsterite, and spinel (analogous to alkali basalts) are close to $Di_{79}CaTs_{20}En_1$ and those in equilibrium with anorthite, forsterite, and pigeonite (analogous to tholeiitic basalt) are close to $Di_{75}CaTs_3En_{22}$. At 7 kbar the equivalent compositions are $Di_{69}CaTs_{28}En_3$ and $Di_{69}CaTs_{26}En_5$ respectively.

In the system CaO–Na_2O–MgO–Al_2O_3–SiO_2, electron microprobe analyses of augites and liquids at 1 bar confirm the changes expected in the loci of liquids and show that the low Na_2O (< 0.50 wt.%) augites are similar to those in CaO–MgO–Al_2O_3–SiO_2. At 7 kbar the orthopyroxene field has expanded sufficiently and augite was not encountered in the limited range of samples studied.

In remelted rocks the augite compositions at 1 bar are similar to the compositions of augites in low pressure effusive rocks. At 2–15 kbar, the available data in the literature for dry basalts show that experimentally recrystallized augites are very sub-calcic and very aluminous, and no natural equivalents exist in plutonic gabbros or in ophiolitic rocks. This discrepancy is not resolved but either the experimental pyroxenes are metastable or the pyroxenes presently in the rocks are not the pristine compositions.

DIOPSIDE solid solutions in the system CaO–MgO–Al_2O_3–SiO_2 at 1 bar are limited to quite small solubilities of enstatite and of calcium tschermakite. New data for these solubilities when liquid is present are presented and compared with a replotting of previous data for the subsolidus solubilities. At higher pressure the solubilities increase and new data at 7 kbar are presented and compared with previous data at 7–15 kbar. Similar data, mostly new but some from the literature, for systems with Na_2O, and with FeO are presented. Finally available data for diopside and liquid compositions in remelted rocks at 1 bar–15 kbar are reviewed. A considerable anomaly exists when the solubilities in the minerals of the rocks are compared with the solubilities determined from the remelted rocks.

Just below the solidus in the system CaO–MgO–Al_2O_3–SiO_2 the range of diopside solid solution increases as pressure increases, as shown by the stippled areas in fig. 1. The diopside compositions can be expressed as solubilities of enstatite (MS) and of calcium tschermakite (CAS) which both lie in the plane of fig. 1 ($CaSiO_3$–$MgSiO_3$–Al_2O_3). Between 1 bar and 7 kbar the An–Di–Fo area shrinks and continues to do so until it vanishes at 9 kbar, where the univariant reaction An + Fo $\rightleftharpoons$ Di + Sp + En occurs (between fig. 1B and C). At about 14 kbar the garnet-forming reaction Di + En + Sp + An $\rightleftharpoons$ Gnt occurs (between fig. 1C and D). Rather similar, if simplified, diagrams along the same lines appear in Stolper (1980*a*) and a more complete pressure–temperature grid appears in Irvine and Sharpe (1982). An X-ray diffraction technique was used to determine diopside compositions in subsolidus experiments in which crystals are seldom larger than 3 μm. Two diffraction peaks were measured and plotted on the grid reported by Benna *et al.* (1981), from which the composition in terms of enstatite and calcium tschermakite solubilities was then read (fig. 2). Microprobe analyses were used to determine the

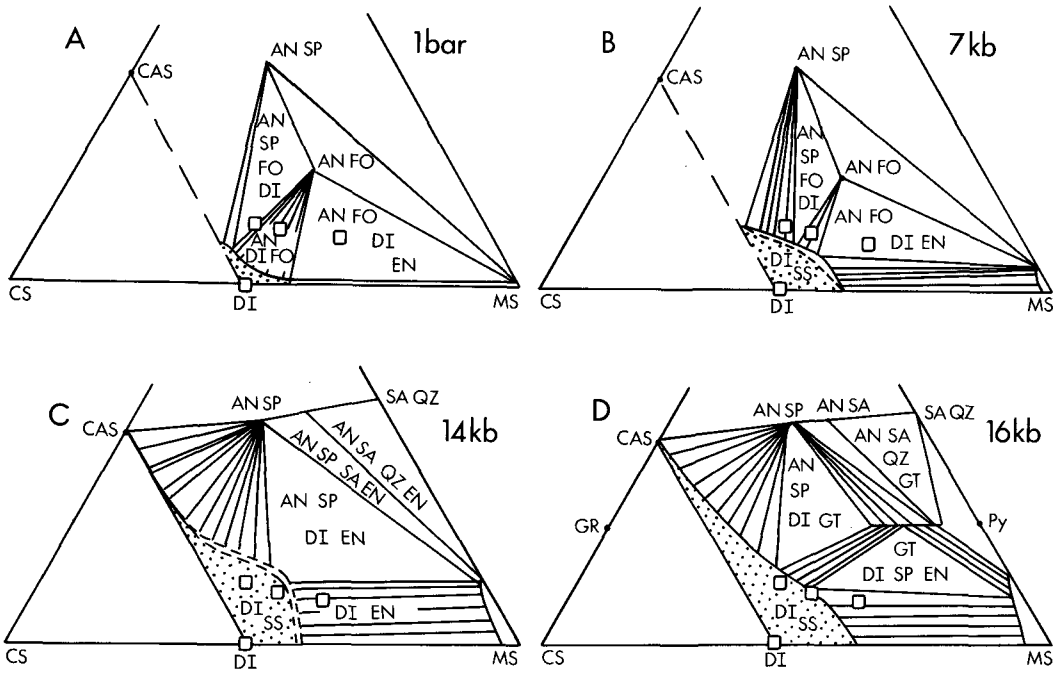

FIG. 1. Schematic subsolidus (about 1200–1300 °C) equilibria in the plane CS–MS–A from 1 bar to 16 kbar, based on Herzberg (1975) to show the broad general changes of the equilibria and of the diopside solid-solution compositions. The squares represent three of the bulk compositions studied and they serve in these and subsequent diagrams as landmarks.

larger crystals present when liquid was present and to determine glass compositions. The bulk compositions studied and the experimental conditions appear in Biggar and Humphries (1981).

The results at 1 bar for the subsolidus are plotted in fig. 3 and define a limit of diopside solid solution shown as the locus E–F, substantially different from previous estimates (Biggar, 1969) as a result of the improvements inherent in the determinative grid of Benna *et al.* (1981).

Results from experiments with liquid present, mostly done between 1968 and 1972 and mostly described and listed in Biggar and Humphries (1981) are shown in fig. 4 from electron microprobe analyses (Table II). The original aim was to confirm the suggestions of Presnall *et al.* (1978) that, at 1 bar, the thermal maximum on An–Di–Fo lies to the silica-rich side of the stoichoimetric plane and to provide some augite–liquid tie-lines for later comparison with similar data for systems with Na_2O and FeO present and for remelted rocks over a range of higher pressures. There are recognized experimental problems in this system as noted by Herzberg (1975). Plagioclase is often present in the starting materials for the experiments and it may require a long time to react. If it persists metastably it prevents the diopside solid solution attaining its equilibrium composition. Diopside solid solutions may be slow to re-equilibrate and Herzberg found that the enstatite content of diopside solid solution was often metastably preserved although the calcium tschermakite's content re-equilibrated in 12 hours. Benna *et al.* (1981) also comment that enstatite-rich diopside solid solutions are slow to re-equilibrate.

Glasses coexisting with forsterite from 1306 to 1286 °C are shown in fig. 4A as filled or half-filled circles. Ideally these should all be coincident with the original bulk compositions H_5 and H_6 which are shown as open squares. The small range observed is some measure of experimental and analytical variation. For the record, coexisting forsterite crystals had CaO contents of 0.89, 0.97, 1.03, and 1.07 wt. %. At 1278 °C and at 1280 °C data for diopside and liquid compositions are shown as triangles. In this and subsequent diagrams symbols with a spike added refer to the assemblage Fo + Di + Lq and normal symbols refer to Fo + Di + An + Lq. Data from Presnall has a *P* attached to it, and a temperature, generally a different and lower

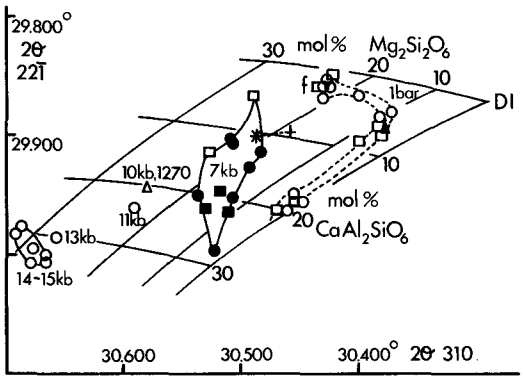

FIG. 2. A plot of 2θ for the pyroxene peaks 221 and 310. The molar grid (moles $Mg_2Si_2O_6$ and $CaAl_2SiO_6$) is taken from Benna *et al.* (1981). For the subsolidus data at 1 bar (Table I) circles are data from Herzberg (1975), squares are data from Biggar (1969), and the filled triangle is a new datum. For the data at 7 kbar, filled circles are data from Herzberg at 1250 °C and squares are new data from runs shown in fig. 6 and Table I at 1300 °C. The open triangle at 10 kbar and 1270 °C is the datum from Herzberg (1975) closest to the invariant An–Di–Fo–Sp–En–Lq; further representative data for augites that are no longer in equilibrium with anorthite and forsterite at 11, 13, and 14–15 kbar are also from Herzberg (1975). The asterisk is the data for a homogeneous pyroxene recrystallized from a bulk composition $Di_{72.7}En_{18.2}CAS_{9.1}$ (molar) called $Di_{90}Py_{10}$ by Herzberg (1975). From the grid, the asterisk gives $Di_{69}En_{20.5}CAS_{10.5}$, and the bulk composition is shown as a plus sign. The difference from the bulk is within the likely accuracy of the grid.

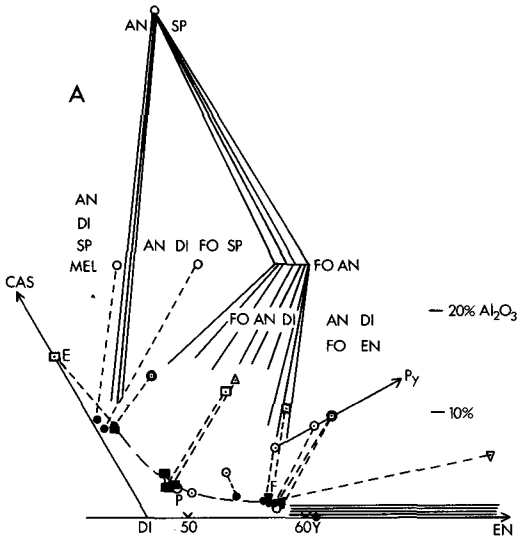

FIG. 3. Detail in the subsolidus at 1 bar of compositions studied (open symbols), and of the diopside solid solutions (filled symbols) determined using the grid of fig. 2. Circles from Herzberg (1975), at 1200 °C, squares from Biggar (1969) and the triangle from the new data. All the X-ray data are reworked to $d_{200}NaCl = 31.718°2\theta$. The points Y, F, and P come from fig. 5 and have liquid present just above the subsolidus and fit well to the subsolidus data.

temperature from that of the isothermal section in which it is plotted and the reasons for this difference are discussed later. Microprobe data at 1274 °C for some diopside and liquid compositions are shown in fig. 4B. The filled triangle is, however, a diopside composition determined by the X-ray method. Fig. 4C at 1264–1263 °C shows microprobe data for diopside and liquid compositions (open diamonds) and determinations of diopside compositions by X-ray diffraction (filled triangles). Close to the CAS join agreement is satisfactory. The enstatite-rich composition determined by X-ray is far removed from the probe analyses and this may be a case of difference (slowness) in equilibration in different samples as mentioned above. The data of fig. 4A–C are combined in a polythermal diagram (fig. 5) to show the locus of liquid composition in equilibrium with plagioclase, forsterite, and diopside.

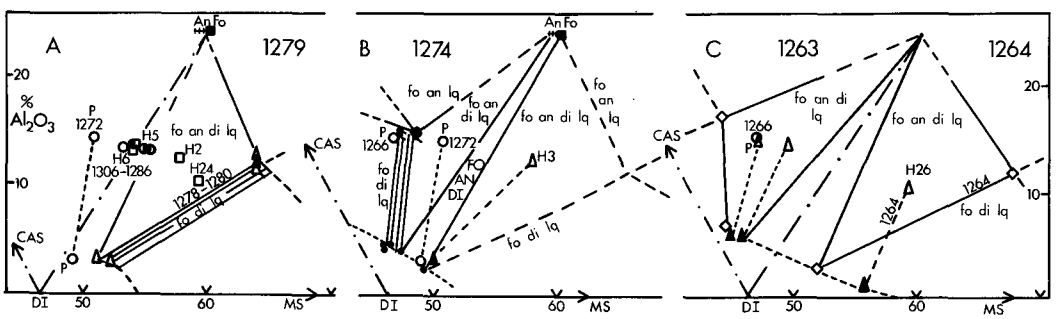

FIG. 4. Data for liquids and for diopside solid solutions from the assemblages Fo + Lq, Fo + Di + Lq, and Fo + Di + An + Lq, projected from forsterite into the plane CS–MS–A. A, B, and C are isothermal sections (except for some polythermal points in A) based on data in Table II.

Table I. X-ray data for clinopyroxene*.

Compn.+				°C	28,221	28,310	Compn.		°C	28,221	28,310
6	3	1	9	1232	29.845	30.421	H	6	1274	29.891	30.378
				‡	29.860	30.423	Py40	Gr60	‡	29.961	30.458
5	3	1	8	‡	29.859	30.432	Py45	Gr55	‡	29.953	30.445
4	3	1	7	1260	29.890	30.383	Di95	Py 5	‡	29.883	30.380
				1252	29.902	30.400	Di90	Py10	‡	29.864	30.397
				1232	29.895	30.377	Di85	Py15	‡	29.868	30.431
				‡	29.880	30.370	Di80	Py20	‡	29.854	30.426
3	3	1	6	1232	29.952	30.455	H	12	1300∫	29.96	30.53
				‡	29.951	30.453	H	9	1300∫	29.96	30.51
2	3	1	5	1228	29.967	30.496	H	5	1300∫	29.94	30.52
					B liquid present						
H	3			1274	29.88	30.39	H	12	1330∫	29.96	30.53
H	26			1264	29.86	30.42	H	9	1330∫	29.97	30.52
H	9			1263	29.92	30.42	H	5	1330∫	29.97	30.55
H	12			1263	29.93	30.42	H	2	1330∫	29.94	30.58
H	2			1300∫	29.91	30.53	H	24	1330∫	29.91	30.54
H	24			1300∫	29.86	30.49					

*Values of 2θ are given for the clinopyroxene peaks 221 and 310, measured relative to d_{200} for NaCl for which the value 31.718° 2θ was used, based on Cu K_α mean radiation of λ = 1.54178. Where necessary previously published data (based erroneously on 31.690° 2θ have been recalculated).

+Molar compositions, in the order MgO-CaO-Al_2O_3-SiO_2, Di for diopside, Py for pyrope H see table II footnote.

‡X-ray data from Herzberg, experiments all at 1200°C

∫at 7kb (others are all at one bar)

There are a few disappointments in figs. 4 and 5. First the diopside solid solution analyses on the enstatite side at 1280, 1278, 1274, and 1264 °C do not fall on a reasonable smooth trend. This could be a slowness to reach equilibrium, as noted above. Secondly, glass analyses could not be obtained from compositions on or close to the stoichiometric divide (the dash-dot line which is the plane An–Di–Fo) at temperatures of 1274 or 1280 °C, because of the small size of the liquid pools. Such analyses should demonstrate that the real divide is, as Presnall shows, to the enstatite-rich side of the stoichiometric plane. Finally, there is a very constant discrepancy in temperature between Presnall *et al.* and this work. Presnall does not state what calibrations he used for his work at 1 bar but quotes 1274 °C for the meeting of the anorthite forsterite diopside liquid fields in the plane An–Di–Fo whereas Biggar and Humphries (1981) quote > 1280 < 1286 °C using a temperature scale, believed to be IPTS-68, although in detail at these temperatures this scale depends on a lithium metasilicate calibration at a presumed temperature of 1208 °C (Biggar, 1972) relative to Au at 1064.5 and diopside at 1395 °C. There is most probably an interlaboratory temperature scale difference of about 6 °C and certainly adding that to Presnall's values, makes the two sets of data in fig. 5 a much better fit. There is no implicit claim here that either temperature is more correct than the other, just an observation that data for liquid compositions can be reconciled by a 6 °C difference.

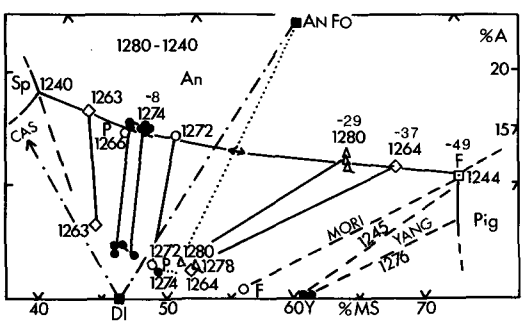

FIG. 5. Polythermal data, from fig. 4, with additional data; F from Mori and Biggar (1981); P from Presnall *et al.* (1978), and Y from Yang (1973).

Other information added to fig. 5 includes liquid, F, and coexisting augite from Mori and Biggar (1981) at 1244 °C, and two augite analyses from Yang (1973) at 1245 and 1276 °C which were in equilibrium with liquids along the olivine-augite-pigeonite field boundary. The points P, F, and Y have already been transferred to fig. 3 to show that

Table II. Augite and glass analyses at one bar.

Phase-Code*	°C	SiO_2	Al_2O_3	MgO	CaO	Total	Products+
GL 30 H 6	1306	49.32	14.61	14.67	20.76	99.57	fo
GL 31 H 6	1292	49.73	15.10	14.06	21.07	100.01	fo
GL 32 H 6	1286	49.69	15.10	13.70	21.10	99.62	fo
GL 35 H 5	1286	48.96	15.63	13.69	21.28	99.58	fo
GL 1 H12	1274	47.01	15.83	12.94	22.65	98.43	fo di
GL 2 H12	1274	47.01	15.87	13.10	23.13	99.11	fo di
GL 91 H12	1274	46.33	15.68	12.86	22.56	97.49	fo di
PX 91 H12	1274	51.38	4.38	18.00	23.50	97.31	fo di
PX 1 H 9	1274	52.68	4.42	17.99	24.41	99.50	fo di an
PX 2 H 9	1274	52.86	4.23	18.20	24.42	99.71	fo di an
GL 3 H 9	1274	47.06	16.15	13.07	22.61	98.89	fo di an
GL 8 H 9	1274	46.94	15.96	12.96	22.59	98.45	fo di an
GL 9 H 9	1274	46.98	16.01	12.92	22.68	98.59	fo di an
PX 6 H 9	1274	52.52	3.96	18.11	23.83	98.42	fo di an
GL 10 H 3	1280	51.08	16.36	12.92	18.17	98.53	fo di an
GL 11 H 3	1280	51.72	15.30	13.26	18.49	98.77	fo di an
PX 94 H 3	1280	52.95	3.04	19.29	22.40	97.68	fo di an
GL 12 H26	1278	51.90	15.01	13.63	18.40	98.94	fo di
PX 8 H26	1278	54.59	2.98	20.36	22.40	100.33	fo di
PX 95 H 3	1274	53.16	2.42	20.32	22.64	98.56	fo di an
GL 92 H11	1263	45.23	16.79	11.84	23.56	97.46	fo di an
PX 4 H11	1263	51.42	6.67	16.75	24.74	99.58	fo di an
GL 13 H26	1264	52.98	15.76	12.84	17.20	98.78	fo di an
PX 97 H26	1264	55.37	2.67	20.48	21.78	98.31	fo di an

*GL for glass, PX for augite, OP for orthopyroxene, H, N, L, A, are starting materials (Biggar & Humphries, 1981, tables I and II) based on An_{100}, An_{67}, An_{50}, An_{33} respectively.

+Liquid (glass) also present in all products, fo for forsterite, di for diopside, an for anorthite, pl for plagioclase, opx for orthopyroxene.

the locus E-F in fig. 3 for augite compositions at 1 bar in the solidus is closely enough the same as the locus just above the solidus.

Diopside compositions at 7 kbar. Phase equilibria of compositions in the plane $CaSiO_3$-$MgSiO_3$-Al_2O_3 equilibrated at 7 kbar and 1300 and 1325 °C are shown in fig. 6. There are two interpretations of the data; fig. 6A (left) assumes that the maximum temperature of An-Fo-Di is above that of An-Di-Fo-Sp and thus that the thermal divide still exists and fig. 6B (right) assumes the opposite. The experimental observations fit both diagrams and

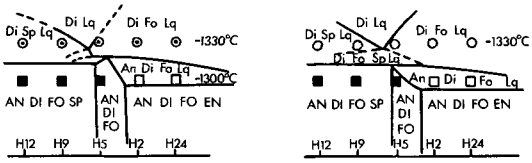

FIG. 6. New experiments at 7 kbar plotted as pseudo-binary diagrams. The compositions are plotted in fig. 7 and some are listed in Biggar and Humphries (1981). Subsolidus samples were soft with crystals up to 3 μm in size; samples with liquids were harder, or even glazed, with crystals generally from 5 to 12 μm.

many more experiments between 1300 and 1325 °C would be required to resolve the real answer (which is another project) which would add little to the knowledge of the diopside compositions. X-ray diffraction data from these experiments (Table I) were plotted in fig. 2 and the compositions of the augites derived from fig. 2, along with some data at 1250 °C from Herzberg, are shown in fig. 7A and B. Fig. 7C shows that the change in diopside composition on freezing is marked for enstatite-rich samples but for the calcium-tschermakite-rich compositions the pyroxene from Di + Sp + Lq at 1330 °C is not distinguishable from the subsolidus pyroxene at 1300 °C.

The change of diopside composition with pressure. A summary of diopside compositions from earlier figures and publications is shown in fig. 8, and it was in fact these data that were used to construct parts of fig. 1. Enstatite and calcium tschermakite both become increasingly soluble at a higher pressure. The band widths at 1 bar, 7 kbar, and 14–15 kbar reflect analytical variation. The band at 1 bar encompasses the data from figs. 3 and 4, the band at 7 kb encompasses the data from fig. 7. At 9 and 10 kbar, close to the invariant point, the filled triangle is the microprobe analysis from Presnall *et*

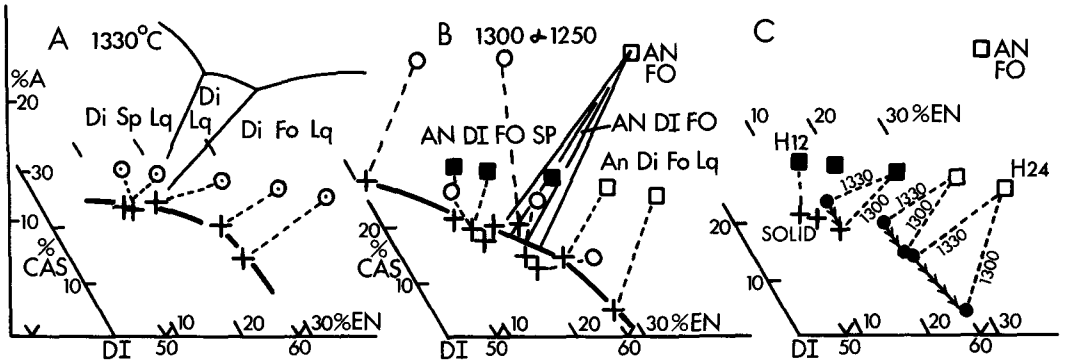

FIG. 7. At 7 kbar, diopside compositions (X-ray) plotted as crosses connected to the bulk compositions from which they crystallized. The bars of the crosses represent a range of about 4 mole % of M_2S_2 and of CAS solubility in diopside, which is probably about the accuracy of the X-ray method. A with liquid present. B, at 1300 °C (squares are starting compositions) three sub-solidus and two with liquid, and at 1250 °C (circles are starting compositions) from Herzberg (1975). C is derived from A and B to show the change in diopside compositions on cooling.

al. (1979) and is reasonably close to Herzberg's point at 10 kbar, 1270 °C, from X-ray diffraction repositioned using the grid of Benna *et al.* (1981). At pressures above the invariant point some representative data for diopside in equilibrium with forsterite, enstatite, and spinel are shown, from fig. 2, and an open diamond from the alumina-free system (Schweitzer, 1982).

Soda-bearing samples

Starting materials were based on three end-member compositions ($An_{67}Ab_{33}$, $An_{50}Ab_{50}$, and $An_{33}Ab_{67}$) chosen to lie in the plane CS–MS–A (when Na_2O is treated according to O'Hara (1976) and calculated as its equivalent of CaO). Phase relations of many of the samples at 1 bar appear in Biggar and Humphries (1981). This present section presents new microprobe data on these 1 bar experiments, and new experiments at 7 kbar with microprobe analyses.

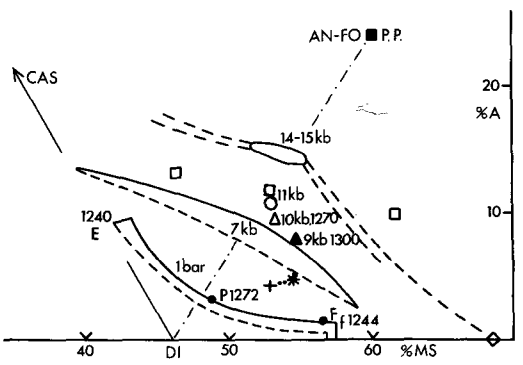

FIG. 8. A summary of diopside compositions from microprobe and from X-ray diffraction from earlier figures.

Selected samples, equilibrated at 1 bar (Biggar and Humphries, 1981 and Humphries, 1975) were analysed by electron microprobe (Table III). Augite and glass analyses are summarized in fig. 9, which confirms the loci of liquid compositions deduced from geometrical relations (Biggar and Humphries, 1981) and which demonstrates augite–liquid tie-lines. The table shows Na_2O contents of augite, from the $An_{67}Ab_{33}$ samples in the range 0.12–0.14 wt. %, and from the $An_{33}Ab_{67}$ samples the values are 0.23, 0.31, 0.36, 0.38, 0.44, 0.55, and 0.60 wt. % of which the last two or three probably represent excitation of glass near the crystal being analysed. *En masse*, the augite analyses in projection (fig. 9) are very close to the Na_2O-free augite compositions of fig. 5.

At 7 kbar, samples with $An_{50}Ab_{50}$ and $An_{33}Ab_{67}$ crystallized orthopyroxene, olivine, and liquid. Although beyond the scope of the title of this paper the results for compositions with $An_{50}Ab_{50}$ are plotted in fig. 10. Those for $An_{33}Ab_{67}$ yield a similar figure which is not published but can be drawn from the data in Table IV. The combined effect of replacing CaO by Na_2O and of increasing the pressure is to enormously expand the orthopyroxene field relative to its extent (as pigeonite) at 1 bar, at the expense of plagioclase and augite. A suggested position for Plag(50:50)–Fo–Di–Opx–Lq is shown as F′ in fig. 10 and this has evolved as a result of pressure and Na_2O changes from the similar point F in fig. 5. A thermal maximum on Plag–Opx–Ol–Lq is inferred. At 1 bar in the system $CaO–MgO–Al_2O_3–SiO_2$, the equivalent equili-

Table III Augite and glass analyses from samples with Na_2O at one bar

Phase-Code*	°C	SiO_2	Al_2O_3	MgO	CaO	Na_2O	Total	Products+
GL 9 N 17	1274	50.21	14.66	12.60	17.72	1.92	97.11	fo di
GL 8 N 17	1274	49.77	14.58	12.40	17.60	1.84	96.19	fo di
PX 9 N 17	1274	52.32	2.64	18.87	23.10	0.14	97.07	fo di
PX 8 N 17	1274	52.67	1.67	19.15	22.92	0.14	96.55	fo di
GL 12 N 22	1274	52.89	14.54	12.72	16.78	1.51	98.44	fo di
GL 13 N 22	1274	52.96	14.40	12.85	16.70	1.51	98.42	fo di
PX 13 N 22	1274	54.40	1.72	20.21	22.26	0.12	98.71	fo di
GL 14 N 21	1260	52.82	15.91	11.65	16.25	1.90	98.53	fo di
GL 17 N 6	1260	50.09	16.64	12.04	18.15	2.13	99.05	fo di
GL 18 N 6	1260	49.52	16.15	12.16	19.09	1.71	98.63	fo di
GL 10 N 3	1251	50.03	16.72	11.28	16.99	2.35	97.37	fo di pl
GL 11 N 3	1251	50.27	16.74	11.41	17.11	2.31	97.84	fo di pl
GL 16 N 6	1251	50.27	16.78	11.16	18.11	2.34	98.66	fo di pl
GL 15 N 9	1251	48.98	17.03	11.36	19.05	2.36	98.78	fo di pl
PX 1 A 6	1222	55.25	2.48	18.59	23.12	0.44	99.86	fo di pl
PX 2 A 6	1222	54.75	2.61	20.26	22.34	0.36	100.32	fo di pl
GL 7 A 6	1222	56.88	18.51	7.59	11.16	6.19	100.33	fo di pl
GL 8 A 6	1222	56.60	18.29	7.59	11.24	6.18	99.89	fo di pl
GL 9 A 18	1234	59.03	16.58	8.37	11.44	4.84	100.25	fo di
PX 10 A 18	1234	56.19	2.40	19.45	21.82	0.55	100.41	fo di
GL 11 A 21	1246	59.62	15.81	8.73	10.73	5.01	99.91	fo di
PX 11 A 21	1246	55.83	1.18	21.67	21.27	0.31	100.26	fo di
GL 14 A 21	1246	59.36	16.13	8.68	10.82	5.06	100.04	fo di
PX 14 A 21	1246	55.24	1.37	20.74	21.71	0.23	99.29	fo di
GL 12 A 21	1234	61.65	16.54	8.06	10.11	5.19	101.54	fo di
GL 15 A 27	1246	58.20	16.14	8.63	11.28	4.68	98.92	fo di
GL 17 A 27	1227	57.89	16.91	8.95	10.75	4.75	99.26	fo di
PX 17 A 27	1227	55.29	1.89	20.57	21.28	0.38	99.42	fo di
GL 42 A 3	1246	57.83	17.77	8.50	10.90	5.09	100.09	fo
GL 41 A 3	1334	58.47	17.65	8.21	10.98	4.88	100.19	fo di
GL 44 A 3	1227	57.80	17.93	7.84	10.81	4.91	99.29	fo di pl
GL 40 A 3	1227	58.38	17.88	7.80	10.73	5.19	99.99	fo di pl
GL 45 A 3	1227	59.06	18.13	7.43	10.33	5.50	100.45	fo di pl

* and + see Table II.

brium also has a thermal maximum (Hytönen and Schairer, 1961).

Iron-bearing systems

Most experimental data for iron-bearing pyroxenes are from the Al_2O_3-free system CaO-MgO-FeO-SiO_2, or if Al_2O_3 is present, from plagioclase-free assemblages and all such data are referenced by Lindsley and Andersen (1983).

Rather surprisingly for the system CaO-MgO-FeO-Al_2O_3-SiO_2 there is only one datum for coexisting augite and liquid from the equilibrium Ol-An-Aug-Lq and it comes from a sample documented in Biggar (1981*a*, fig. 8) although the augite and liquid analyses were determined by Humphries (pers. comm.). The sample at 1105 °C is very close to also having pigeonite present, and the augite and liquid are plotted in fig. 9 as filled triangles. As expected from the behaviour of augites in the pyroxene quadrilateral, the presence of iron (filled triangle in fig. 9) leads to a much greater enstatite plus ferrosilite solubility than in the magnesian system (open triangle). Fig. 9 is also used to summarize the positions of points of the type F. In CaO-MgO-Al_2O_3-SiO_2 (open triangle) F is at 1244 °C and −49% olivine. When MgO is replaced by 0.75FeO 0.25MgO, F (filled triangle) is less than 1105 °C and is closer to olivine at −20%. When CaO is replaced by Na_2O such that the feldspar is $An_{33}Ab_{67}$ a guess (from data in Table IV) can be made that F′ is below 1200 °C and further from olivine at about −60%. All accord with the known expansion and contraction of the olivine versus plagioclase fields (Biggar, 1983).

Clinopyroxene and liquid compositions in rocks remelted at 1 bar

Data Presentation. Available augite compositions and coexisting glasses or whole rocks are presented in a form resembling the presentation

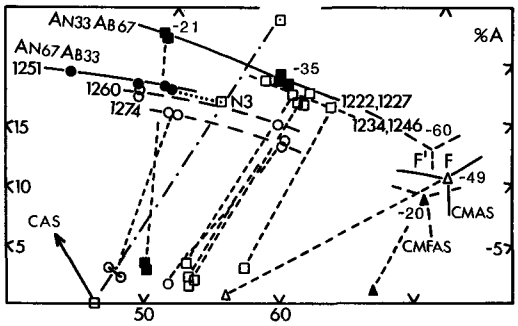

FIG. 9. Augite and glass analyses (Table III) at 1 bar, from the soda-bearing system projected from forsterite into CS-MS-A. The experimental products from the assemblage Fo-Di-Lq are shown as open symbols and dashed lines and from the assemblage Fo-Di-Plag-Lq as filled symbols and full lines. Data for compositions with $An_{67}Ab_{33}$ are shown as circles, yielding contours at 1274 and 1260 °C on the Fo-Di-Lq surface, and a contour at 1251 °C on the Plag-Fo-Di-Lq surface. The dotted line from the bulk composition N3, in the stoichiometric plane, connects to glass in that sample at 1251 °C and thus the thermal divide along Plag-Fo-Di-Lq must still be to the right (silica-rich) side of N3. When data for compositions based on $An_{33}Ab_{67}$ (shown as squares) are examined in detail, there are some problems possibly due to loss of Na_2O from the glass, but the data as shown are still of reconnaissance value in confirming the position of the cotectic surface shown by contours at 1234 and 1246 °C (coincident in the figure) and at 1222 and 1227 °C (coincident), and in giving augite compositions.

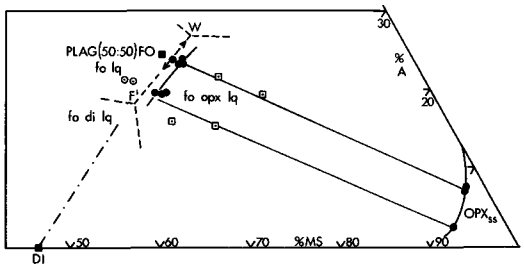

FIG. 10. Orthopyroxene and glass analyses from soda-bearing (An_{50}) samples at 7 kbar, 1300 °C, which yielded olivine, orthopyroxene and liquid projected from M_2S into CS-MS-A and used to suggest the location of the Plag-Ol-Opx-Lq boundary from F to W. The expansion of the orthopyroxene field is seen by comparison with fig. 5, where the equivalent of the point F is at 1244 °C.

just given for the synthetic systems by reducing and projecting the data (O'Hara, 1976) such that Fe and Mg are combined and pyroxenes then represented as three apices Jadeite + Calcium tschermakite; Diopside + Hedenbergite; Enstatite + Ferrosilite. Pyroxenes stoichiometric with respect to Di-Cats-En will lie in the plane CS-MS-A. This projection into CS-MS-A is suitable to compare pyroxenes over a limited range of Fe : Mg when Al, Na, Ti, and Cr are important variables. Analytical errors, and non-stoichiometry, result in compositions which lie off the plane. These are projected back on to the plane from olivine. The olivine height is some measure of the acceptability of the pyroxene analyses, zero height representing stoichiometry. Heights are shown, with comments, in many diagrams, but absolute values depend on knowing Fe^{2+} and Fe^{3+} separately, as with any recasting of a pyroxene analyses, to test its acceptability.

Before examples of this projection are shown a very similar A-C-FM diagram as used by Thompson (1974) to plot some high pressure remelted pyroxenes is reproduced in fig. 11A. His remarks about the particular convention used for calculating pyroxene end-members from oxide analyses remain apposite and account for some of the differences between his A-C-FM diagram and the olivine projection into CS-MS-A. Parts of two of Thompson's trends from fig. 11A are reproduced in fig. 11C.

To further guide the reader from more familiar ground into this CS-MS-A projection, data for the Skaergaard and for the Quairading intrusions, shown in the traditional quadrilateral in fig. 11B are plotted in projection in fig. 11C. In these layered intrusions the Fe enrichment is accompanied by gradual falls in Al_2O_3 and TiO_2 shown in fig. 11C as slight falls in the lines *a*-*b*-*c* and *d*-Q. The break at *b* in fig. 11B at which the pyroxene ceases to become more sub-calcic is reflected in fig. 11C by an acute bend back towards more calcic compositions.

Experimental limitations. Most experimental data are from tholeiites which recrystallize to olivine and plagioclase followed by augite. The extent of crystallization increases very rapidly when these three phases co-crystallize (up to 50% crystallization for a temperature drop of 20 °C; Biggar, 1983). The augite crystals are often small and may be partially unreacted relicts from the starting material, since run lengths are often short relative to the time it is likely to take an augite to re-equilibrate. These problems show up, typically, as mg numbers which are erratic as temperature drops, and in other irregularities in minor element contents (Cr_2O_3, TiO_2, and Na_2O) with temperature or pressure.

Augites and liquids from Scottish Midland Valley Basalts. A very extensive data set of augite and liquid analyses from experimentally remelted Carboniferous basalts at one bar with olivine and plagioclase also present is available (D. G. Russell, pers. comm.). Individual treatment of the data for each sample is given by Russell (in preparation) and

Table IV. Orthopyroxene and glass analyses at 7kb, 1300°C

Phase-Code*	SiO_2	Al_2O_3	MgO	CaO	Na_2O	Total	Products+
GL 7 L23	55.23	22.52	9.70	7.46	5.28	100.18	ol opx
GL 8 L23	55.08	22.51	9.94	7.52	5.08	100.11	ol opx
OP 8 L23	55.72	7.46	35.92	0.99	0.08	100.16	ol opx
GL 15 L27	56.32	23.42	7.80	7.04	5.62	100.20	ol opx
GL 16 L27	56.51	23.91	8.17	7.07	5.61	101.27	ol opx
OP 16 L27	55.41	7.48	36.19	0.87	0.08	100.02	ol opx
GL 10 L 3	53.55	19.91	9.13	12.77	4.13	99.49	ol
GL 11 L 3	53.31	19.60	10.32	12.38	3.90	99.50	ol
GL 12 L24	55.21	19.50	9.55	11.90	3.91	100.07	ol opx
GL 13 L24	54.68	18.56	11.04	11.61	3.76	99.65	ol opx
GL 14 L31	54.76	18.14	10.93	11.65	3.93	99.41	ol opx
OP 14 L31	58.10	2.67	36.72	2.61	0.06	100.16	ol opx
GL 1 A 2	56.69	18.14	10.12	9.53	5.34	99.82	ol
GL 2 A 2	56.74	17.99	10.00	9.50	5.34	99.57	ol
GL 3 A20	57.25	17.89	9.87	9.46	5.34	99.82	ol opx
OP 1 A20	57.92	1.72	35.60	3.42	0.14	98.80	ol opx
OP 2 A20	56.04	3.18	34.91	2.79	0.25	97.17	ol opx
GL 4 A20	57.22	18.00	9.69	9.60	5.31	99.82	ol opx
OP 5 A25	57.97	3.23	36.63	1.73	0.31	99.69	ol opx
GL 5 A25	58.12	20.05	8.28	8.29	5.60	100.34	ol opx
OP 6 A25	58.43	2.43	36.66	2.37	0.09	99.98	ol opx
GL 6 A25	58.13	20.56	7.52	8.15	5.57	99.93	ol opx

* and + see table II

fig. 12 is a generalized diagram. Arrows showing liquid evolution fall away from the dashed line at *a*, liquids to the left of the dashed line become more nepheline normative as temperature falls, and those to the right more silica normative. Liquids near E have olivine heights of +10% but towards F the liquids pass through the plane, becoming more siliceous, being −10% near *a* and −57% near F. Liquids to the left have mg values of 62–45, those to the right have 53–37.

The augite compositions occupy a broad band, but all those above the dashed line had olivine heights from −4 to −11 suggesting contamination of the analysed spot by glass so that the range of acceptable augite compositions is below the dashed line. The TiO_2 content of the augites changes, with some overlap, from 3.8 wt. % to 0.7 wt. % as shown. There is evidence that the experimental augite crystals are not as homogeneous as expected and one deduces that 20 h is insufficient to equilibrate the crystals even in starting materials ground to less than 10 μm. Cr_2O_3, which had been accidentally added to all the samples during crushing sometimes reached high levels (1.2 wt. %) in the augite crystals and sometimes remained low, suggesting uneven growth and diffusion. To a very large extent the augite compositions in the remelted samples and in the rock as loaded overlapped so the experiments do not tell us whether the augites did not need to re-equilibrate, or did not have time to equilibrate (contrast with data for Réunion, see later). Relative to iron-free pyroxenes (fig. 3) these ion-bearing ones are displaced to greater Al_2O_3 and greater enstatite contents.

Augite and liquids from other studies at 1 bar. A selection of data from remelted rocks at 1 bar with augite and liquid present along with plagioclase and forsterite is plotted in fig. 13. These data for augites and for liquids are a reasonable match to those of Russell (fig. 12). In detail the data are for two ocean tholeiites (filled circles) from Walker *et al.* (1979) and for two other ocean tholeiites (open squares) from Biggar and Kadik (1981), for alkali basalts (as plus signs) from Boivin (1980), and for a high-alumina basalt (open circles) from Grove *et al.* (1982). The field boundary with arrows comes from geometrical considerations of experiments on chilled margins (Biggar 1974).

Some authors expressed reservations about their augite analyses. Kadik (pers. comm.) noted that his augites were probably relicts inherited from the rock powder loaded. Walker *et al.* (1979) noted inhomogeneous augites, and observed gradients in FeO content extending less than 5 μm into a crystal for runs of 12–22 h duration. None of the authors studied augite compositions sufficiently, relative to the augite present in the powdered rock, to say much about its re-equilibration, although Grove's experiments were as long as 542 h. As with Russell's data, there is more TiO_2 (2.7–3.5%) and more

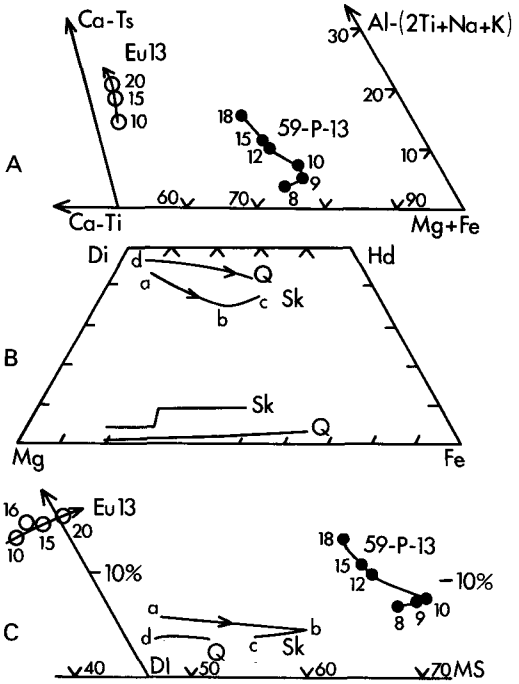

FIG. 11A. The A–C–FM diagram used by Thompson (1974, fig. 8) to plot pyroxenes from remelted rocks, showing two of his samples. B shows natural pyroxenes from the Skaergaard intrusion (Brown, 1957) and form the Quairading intrusion Davidson (1968) plotted in the pyroxene quadrilateral. C shows the olivine projection into CS–MS–A used to plot the pyroxenes of the above figures. The trends for EU13 and for 59-P-13 from Thompson show the resemblance of the olivine projection to the A–C–FM diagram but in detail there are differences, such as in the position of augites from the augite-leucitite, EU13, as measured relative to the join diopside–calcium-tschermakite, and less obvious, but still large differences in the 'enstatite' content of augites from the olivine tholeiite 59-P-13, due to differences in the calculation procedures.

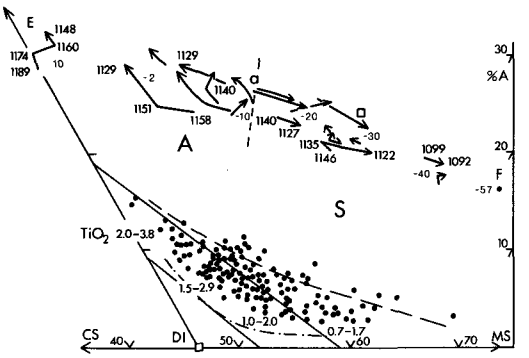

FIG. 12. Projection from Fo into CS–MS–A of the data of Russell (pers. comm.) for augite and liquids at 1 bar with olivine and plagioclase also present. The dash dot line is for Fe-free pyroxene from fig. 3.

Na_2O (0.6%) in the augites from the alkalic samples than in those from the tholeiites (0.6–0.7% TiO_2) and 0.2% Na_2O. The above experiments were aimed at producing equilibrium results, in contrast to the final set of data, replotted in fig. 13 which were obtained by Schiffman and Lofgren (1982) in cooling rate experiments. Such experiments yielded subcalcic augites (open triangles) which became increasingly aluminous as the cooling rate increased from 1 to 120 °C per hour (the cooling rates are shown as values from 1 to 120 in the figure).

Augite compositions in some low-pressure, eruptive rocks

There are in the literature many thousands of analyses of augite from low-pressure and erupted rocks, and many of these have been grouped and reviewed by Leterrier *et al.* (1982) in nine categories. Mean values from Leterrier are plotted in fig. 14, as the filled circles numbered 1 to 9. In each case the circle at the left is when all iron is calculated as Fe^{2+}, and the circle at the right is for 25% of the iron as Fe^{3+}. 1 is for intracontinental high alkali basalt, 2 for oceanic island high alkali, 3 for intracontinental moderate alkali, 4 for oceanic island moderate alkali, 5 for continental calc-alkali, 6 for non-orogenic transitional tholeiite, 7 for island arc tholeiite, 8 for island arc calc-alkali, and 9 for abyssal MORB.

As a further example of the normal range of augite compositions from a suite of eruptive rocks the groups A and B from Sigurdsson (1981) are shown as open circles. These were phenocrysts in rocks, with very low phenocryst contents such that the bulk rock analyses (also shown) probably represent a liquid analyses. Group A is more

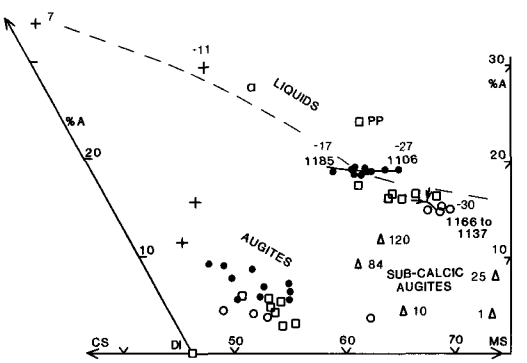

FIG. 13. Experimental data for augite and liquid compositions (microprobe) in remelted rocks at 1 bar, with olivine and plagioclase also present.

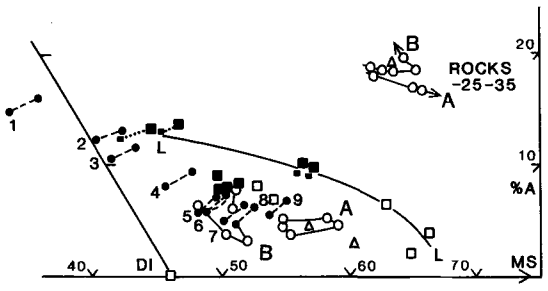

FIG. 14. Augite compositions in some low pressure eruptive rocks. The symbols 1-9 are mean values from 700 augite compositions in basalts reviewed by Leterrier *et al.* (1982).

Fe-rich and as expected (figs. 9 and 11) has a higher En + Fs content which plots in this figure at higher MS values. The bulk rocks plot in a very similar position to the experimental liquids of fig. 13. Triangles are from Jakobsson *et al.* (1978) for a similar very glassy rock.

Beyond this normal range, a search revealed some extremes of augite compositions from ocean basalts. The most aluminous, and least calcic examples found in the literature were those from Bence *et al.* (1975) from the Caribbean shown as open squares (microprobe analyses, with all iron expressed as FeO) and those from Muir and Tilley (1964) from the mid-Atlantic (wet chemical analyses) shown as filled squares for the analyses as reported and connected to smaller squares to represent recalculation to all iron as FeO. Based on these data the curve L–L is proposed as an extreme limit of augite compositions in erupted basalts, and the data of Leterrier can be taken as the mean.

When the augite compositions in the remelting experiments at 1 bar (figs. 12 and 13) are compared with the means, and even with the extremes found in rocks there is considerable broad general agreement. For steady temperature experiments, and for phenocrysts in rocks, the augite compositions are not too aluminous and not too rich in MS component. They lie between the diopside apex and the curve L–L. Only for cooling rate experiments (1 to 120 °C per hour, fig. 13) does an aluminous, but particularly a sub-calcic pyroxene grow, equivalent to the groundmass pyroxenes found in so many effusive basalts which probably cool at similar rates.

Clinopyroxene and liquid compositions in rocks remelted at pressure

Augites and liquids from basalts from Réunion remelted at $2\frac{1}{2}$ to 10 kbar. Remelting studies (M. Fisk, pers. comm.) of rocks from Réunion give information about augites and liquids from 2.5 to 10 kbar. Samples in general were pre-reduced at the Fe-wüstite buffer and subsequently held for 2–48 h in molybdenum capsules. The run products contained very little Fe^{3+}. The starting material was rock, ground up so that very few fragments were as large as 10 μm. In some experiments the powders were brought up to temperature and held. In others the samples were superheated to reduce or even destroy crystal nuclei and cooled 20 to 50 °C to be held at the run temperature. The pyroxenes in the experiments often differed markedly from those in the rocks.

The original basalt contained two types of augite phenocrysts shown as groups A and B with distinct TiO_2 contents and distinct Mg/(Mg + Fe) ratios as shown in fig. 15B. The experiments contained augites which sometimes plotted as close clusters and these are arbitrarily labelled D, G, and H. Each of these narrow ranges is actually less homogeneous than it appears because the coefficient of variation for each element in the analyses (sigma divided by the mean, compare Biggar, 1981*b*) is from 5 to 8% whereas glasses in the same charge had coefficients below 3%, even for Na_2O. This suggests genuine chemical zonation or ranges within the augite crystals. Other experiments which, to avoid confusion, are not plotted, gave a large range of augite compositions from the original, near A and B, towards the groups D, G, and H. This span or inhomogeneity was related neither to run duration, nor to overshoot, nor to up-to-temperature, and suggests that in such experiments augites of several origins were caught in a state of reaction which was not complete. The groups D, G, and H clearly grew during the experiments, and are markedly different from those in the rocks. This contrasts with the less determinate behaviour in Russell's work at 1 bar.

The composition of liquids in equilibrium with augite, plagioclase, and olivine varies with pressure as shown in projection in fig. 15A, and as a simpler variation diagram (fig. 15C) of CaO *vs.* MgO in which such liquids are joined by double lines. Liquids at higher pressures are less calcic for a given MgO content. These data are the first, experimentally, on one basalt in the pressure range 2.5 to 10 kbar, to reveal the effects of pressure on the cotectic liquid (Fisk, in prep.).

Augites in other dry experimental charges at 2 to 15 kbar are very sub-calcic augites. The individual points are plotted in two figures (16 and 17) along with ranges representing natural pyroxenes from other parageneses (e.g. see Wass, 1979). The area GLP represents pyroxenes in gabbros, lherzolites, and peridotites from close to the petrological moho

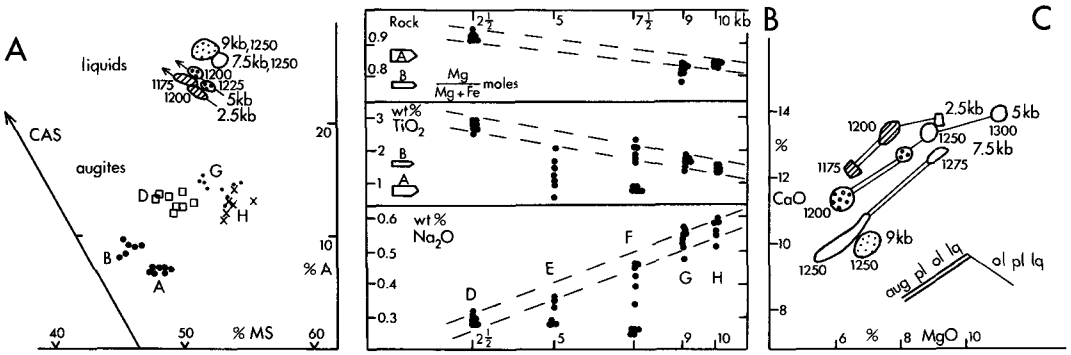

FIG. 15A. Projection from olivine into CS–MS–A of selected augites and liquid from a basalt and from remelted samples of the basalt, data from M. Fisk. B. Molar Mg/(Mg + Fe), wt. % TiO_2, and wt. % Na_2O in analysed augite crystals from the original rock (A and B) and from selected experiments at 2.5–10 kbar. D, G, and H were selected because the augite compositions were tightly clustered. Other experiments gave a range of analyses, E and F being typical. The dashed lines are based on the experiments D, G, and H which are interpreted as approaching equilibrium. It appears that in experiments such as E and F augites range from the original, as loaded, towards an equilibrium composition. C. CaO *vs.* MgO variation diagram for liquid compositions in the cotectic equilibrium with augite, plagioclase, and olivine shown joined by double lines. Liquids in equilibrium with fewer phases are joined by single lines.

in ophiolites. The mg number of these pyroxenes is about 90. The area Al-Aug represents aluminous augite megacrysts with mg number about 75.

Interpretation of the experiments at 2 to 12 kbar is not satisfactory. Steady temperature experiments yield very sub-calcic augite with mg number generally from 80 to 90. (Except for a calcic augite from Takahashi and Kushiro (1983) at 8 kbar and 1200 °C, which is so far removed from all other data that it seems improbable that it can be correct.) It is regarded as only coincidental that these sub-calcic augites resemble pyroxenes from 1-bar cooling-rate experiments. In contrast, in rocks which are judged to have crystallized at elevated pressure, such as gabbros and ophiolites, the augite is calcic, and in some suites also aluminous. This discrepancy suggests that either the high-pressure *dry* experiments

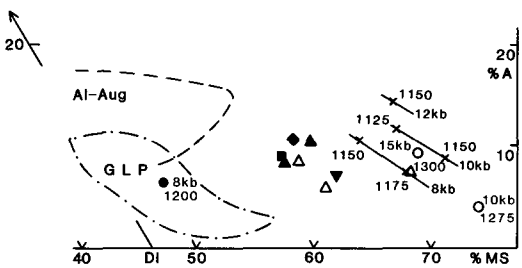

FIG. 16. Augite compositions from dry remelted basalts, peridotites, and 'pyrolites'. Filled symbols, up to 12 kbar, when olivine, plagioclase, sometimes orthopyroxene, and liquid were present or judged to be close to present. Open symbols at higher pressures, 12–15 kbar, when spinel and enstatite were present or nearly present. Triangles, 12 kbar, 1290 and 1305 °C, and 15 kbar, Green *et al.* (1979); circles, Takahashi (1980) and Takahashi and Kushiro (1983); inverted triangles, 10.5 kbar, 1290 °C, Fujii and Bougault (1983); square, 10 kbar, 1250 °C, Stolper (1980*b*); diamond, 8 kbar, 1250 °C, Bender *et al.* (1978); crosses, Thompson (1974 and 1975).

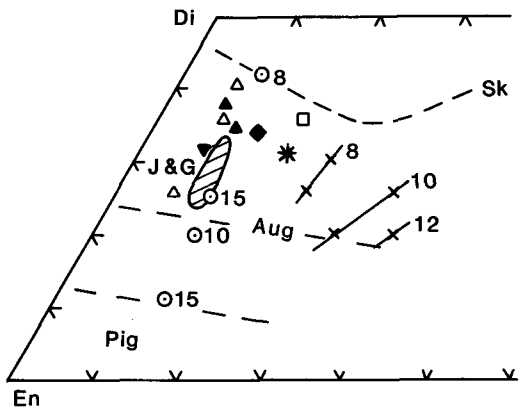

FIG. 17. The pyroxene quadrilateral with much the same data as fig. 16 but with the addition of the following; the area J and G from Jacques and Green (1980) who report a very limited range of sub-calcic augite compositions from experiments at 2, 5, 10, and 15 kbar (usually without plagioclase and with various other coexisting phases) over a relatively large temperature range from 1100 to 1350 °C, with no obvious pattern of pyroxene composition related to pressure or temperature; the dashed line for the Skaergaard trend; and the asterisk (Green and Ringwood, 1967) which is an augite in an alkali olivine basalt at 9 kbar with only olivine and liquid as coexisting phases—it is very sub-calcic, given the nature of the starting material.

have nucleated, grown, and retained a metastable sub-calcic augite composition, or that the rocks originally crystallized such a sub-calcite augite and lost it without textural trace by retrograde reactions during cooling and depressurization. Wilkinson and Taylor (1980) restate that cognate megacryst populations may delineate high-pressure fractionation trends for alkali basalts and note that evidence about high-pressure crystallization of tholeiitic magmas is limited; they describe one suite of pyroxenites, lherzolites, and granulites, interpreted as fragments of a layered tholeiitic pluton and further suggest that small amounts of water somewhat suppress plagioclase crystallization leading to a more calcic augite than, for example, in Bender's experiments. Wilkinson and Taylor recognize the possibility of the former existence of sub-calcic augites and that recrystallization has modified the pristine pyroxenes. Certainly in experiments with water present up to 10 kbar (Green, 1973; Helz, 1973) the augites are more calcic.

One petrological conclusion which depends on the composition of the augite in 10 kbar experimental runs is that of Stolper (1980*b*). In his fig. 7 he shows that the direction of falling temperature along the plagioclase-augite-olivine liquid field boundary is from tholeiitic towards alkalic for most experimental data (much the same data as in figs. 16 and 17). If the high pressure dry experiments have yielded a metastable sub-calcic augite then the conclusion will not apply to natural differentiation in tholeiitic plutons, if no such sub-calcic augite ever crystallized in them. If the rocks, on the other hand, have lost their original augite, then using the retrograded augite for daughter liquid and extract calculations will give conclusions which do not apply to natural differentiation.

The nature of the augite-liquid tie-lines is illustrated in fig. 18 compounded from figs. 13 and 16 with the addition of some of the available data for liquids at 9-10 kbar, and at 15 kbar. The augite-liquid tie-lines swing quite markedly. As pressure increases the liquids become more alkalic and the augites become more sub-calcic such that at 15 kbar the surprise is that the augite with the greatest solubility of enstatite in it (which at 1 bar would be recognized as super-tholeiitic, or within the forbidden zone) is in equilibrium with an alkali olivine basaltic liquid. The liquids actually change rather less in composition than do the pyroxenes.

Petrologists need to search more carefully for evidence that pyroxenes now observed in deep-seated tholeiitic rocks (and perhaps alkalic rocks) have retrograded, and experimental petrologists need to account more confidently for the sub-calcic augites in their products. The process of granule

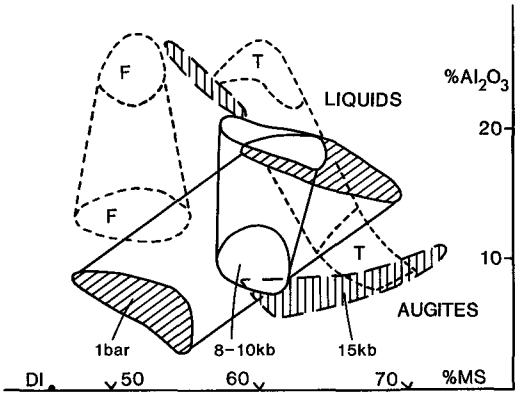

FIG. 18. Coexisting augite and liquids; at 1 bar for ocean tholeiites from fig. 13; at 8-10 kbar for ocean tholeiites from Bender *et al.* (1978), Stolper (1980*b*) and Fujii and Bougault (1983); at 2.5-9 kbar for basalts from Réunion, F, from fig. 15; at 8-12 kbar for transitional basalts from Skye and Snake river (Thompson, 1974, 1975); and at 14-15 kbar for peridotite-basalt sandwiches from Takahashi and Kushiro (1983).

exsolution recently proposed by Lindsley and Andersen (1983) and their similar comments on the discrepancies between natural and experimental data, in their case for two pyroxene assemblages, lead to very similar conclusions as those from the data discussed in this paper, for augite, plagioclase, olivine assemblages (figs. 16, 17, and 18). Together the two papers probably encompass most of the literature and reinforce each other.

REFERENCES

Bence, A. E., Papike, J. J., and Ayuso, R. A. (1975) *J. Geophys. Res.* **80,** 4775-804.
Bender, J. F., Hodges, F. N., and Bence, A. E. (1978) *Earth Planet. Sci. Lett.* **41,** 277-302.
Benna, P., Bruno, E., and Facchinelli, A. (1981) *Contrib. Mineral. Petrol.* **78,** 272-8.
Biggar, G. M. (1969) *Progr. Exptl. Petrol.* **1,** 97-104.
——(1972) *Mineral. Mag.* **38,** 768-70.
——(1974) *Contrib. Mineral. Petrol.* **46,** 159-67.
——(1981*a*) *Bull. Minéral.* **104,** 375-80.
——(1981*b*) *Progr. Exptl. Petrol.* **5,** 96-8.
——(1983) *Mineral. Mag.* **47,** 161-76.
——and Humphries, D. J. (1981) Ibid. **44,** 309-14.
——and Kadik, A. A. (1981) *Progr. Exptl. Petrol.* **5,** 122-6.
Boivin, P. (1980) *Bull. Minéral.* **103,** 491-502.
Brown, G. M. (1957) *Mineral. Mag.* **21,** 511-43.
Davidson, L. R. (1968) *Contrib. Mineral. Petrol.* **19,** 239-59.
Fujii, T., and Bougault, H. *Earth Planet. Sci. Lett.* **62,** 283-95.
Green, D. H. (1973) Ibid. **19,** 37-53.

Green, D. H., Hibberson, W. O., and Jacques, A. L. (1979) In *Petrogenesis of mid-ocean ridge basalts* (McElhinny, ed.). Academic Press, London.

——and Ringwood, A. E. (1967) *Contrib. Mineral. Petrol.* **15,** 103–90.

Grove, T. L., Gerlach, D. C., and Sando, T. W. (1982) *Contrib. Mineral. Petrol.* **80,** 160–82.

Helz, R. T. (1973) *J. Petrol.* **14,** 249–302.

Herzberg, C. T. (1975) *Phase assemblages in the system CaO-Na_2O-MgO-Al_2O_3-SiO_2 in the plagioclase-*lherzolite and spinel-lherzolite mineral facies. Ph.D. thesis, Edinburgh.

Humphries, D. J. (1975) *Phase equilibrium studies of some basalt-like compositions in the system CaO-MgO-Al_2O_3-Na_2O-Fe-O_2.* Ph.D. thesis, Edinburgh.

Hytönen, K., and Schairer, J. F. (1961) *Carnegie Inst. Wash. Yearb.* **60,** 125–41.

Irvine, T. N., and Sharpe, M. R. (1982) Ibid. **81,** 294–303.

Jacques, A. L., and Green, D. H. (1980) *Contrib. Mineral. Petrol.* **73,** 287–310.

Jakobsson, S. P., Jonsson, J., and Shido, F. (1978) *J. Petrol.* **19,** 669–705.

Leterrier, J., Maury, R. C., Thonon, P., Girard, D., and Marchal, M. (1982) *Earth Planet. Sci. Lett.* **59,** 139–54.

Lindsley, D. H., and Andersen, D. J. (1983) *J. Geophys. Res.* (Suppl. 13th Lunar Sci. Conf.) **88,** A887–A906.

Mori, T., and Biggar, G. M. (1981) *Progr. Exptl. Petrol.* **5,** 144–5, 147.

Muir, I. D., and Tilley, C. E. (1964) *J. Petrol.* **5,** 409–34.

O'Hara, M. J. (1976) *Prog. Exptl. Petrol.* **3,** 103–26.

Presnall, D. C., Dixon, J. R., O'Donnell, T. H., Brenner, N. L., Schrock, R. L., and Dycus, D. W. (1978) *Contrib. Mineral. Petrol.* **66,** 1232–41.

————————and Dixon, S. A. (1979) *J. Petrol.* **20,** 3–35.

Schiffman, P., and Lofgren, G. E. (1982) *J. Geol.* **90,** 49–78.

Schweitzer, E. (1982) *Am. Mineral.* **67,** 54–8.

Sigurdsson, H. (1981) *J. Geophys. Res.* **86,** 9483–502.

Stolper, E. (1980*a*) *Geochim. Cosmochim. Acta* (Suppl. 11th Lunar Sci. Conf.), 235–50.

——(1980*b*) *Contrib. Mineral. Petrol.* **74,** 13–27.

Takahashi, E. (1980) *Carneg. Inst. Wash. Yearb.* **79,** 271–76.

——and Kushiro, I. (1983) *Am. Mineral.* **68,** 859–73.

Thompson, R. N. (1974) *Mineral. Mag.* **39,** 768–87.

——(1975) *Contrib. Mineral. Petrol.* **52,** 213–32.

Walker, D., Shibata, T., and De Long, S. E. (1979) Ibid. **70,** 111–25.

Wass, S. Y. (1979) *Lithos* **12,** 115–32.

Wilkinson, J. F. G., and Taylor, S. R. (1980) *Contrib. Mineral. Petrol.* **75,** 225–33.

Yang, H.-Y. (1973) *Am. J. Sci.* **273,** 488–97.

[*Manuscript received 14 July 1983; revised 16 December 1983*]